# CHAPTER 4

# RESULTS AND DISCUSSION

## 4.1 Validation of spectrofluorometric method

### 4.1.1 Calibration curve for standard salbutamol sulfate

Example of standard curve of salbutamol sulfate is shown in Figure 4.1. The calibration curve was prepared daily. In this case, correlation coefficient is above 0.999 in the range of 0.2-2.0 µg/ml.

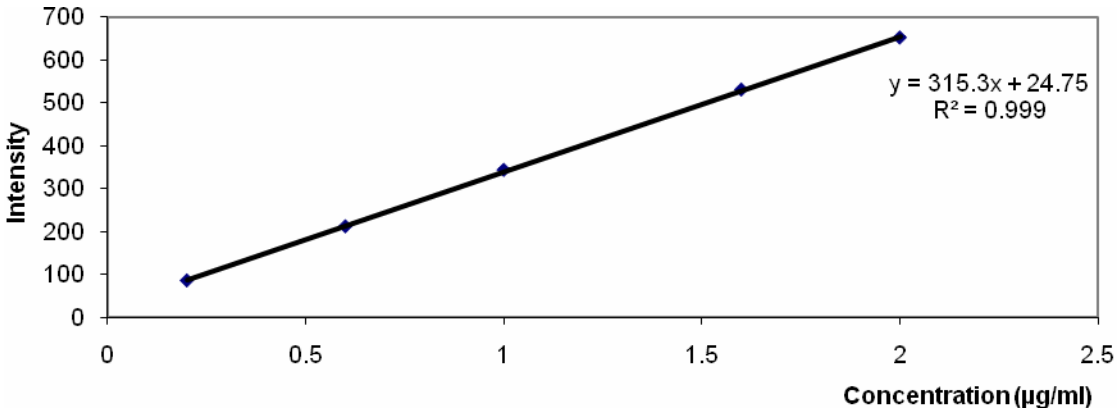


Figure 4.1 Standard curve of salbutamol sulfate

### 4.1.2 Method validation of salbutamol sulfate

Figure 4.2 and 4.3 show the intra-day and inter-day precision of salbutamol sulfate. In figure 4.2 the %RSD of salbutamol sulfate is not higher than 2% in all concentrations in this study. When we considered inter-day variation (Figure 4.3), the results show that the %RSD was between about 3 and 5. Therefore, the results reveal that the analytical method is acceptable for

analysis of samples both intra-day and inter-day. Both intra and inter-day data were shown acceptable precision. Thus, the analysis of salbutamol sulfate was more precise when the sample was analyzed in the same day (%RSD<2).

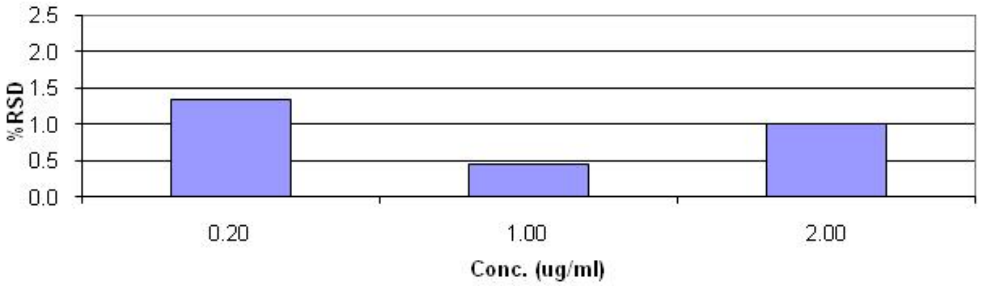


Figure 4.2 Intra-day precision of salbutamol sulfate

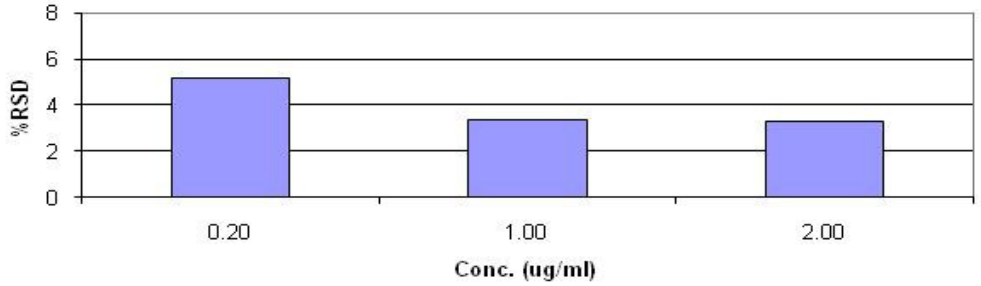


Figure 4.3 Inter-day precision of salbutamol sulfate

Table 4.1 shows that salbutamol sulfate have high accuracy. At concentration 0.2-2 µg/ml, the %recovery of salbutamol sulfate is over 95 with standard deviation less than 2. The results suggest the analytical is accurate.

Table 4.1 Intra-day and inter-day accuracy of salbutamol sulfate (mean±SD, n=5)

| Concentration µg/ml | Intra-day | Inter-day |
|---|---|---|
| 0.20 | 98.39 ± 1.85 | 98.83 ± 1.94 |
| 1.00 | 101.96 ± 0.50 | 102.70 ± 2.37 |
| 2.00 | 99.78 ± 1.05 | 100.14 ± 1.42 |

## 4.2 Formulation design and devices evaluation

### 4.2.1 Particle size distribution of DPI formulations

Three collected carrier size ranges have their volume median diameters about 18, 29 and 65 µm as shown in Table 4.2. The example of volume particle size distribution of lactose collected from sieve 30-71 µm is shown in Figure 4.4. In this study, all of three collected carriers have span more than 1.2, these appear that each collected carrier have poly-disperse size distribution. All of collected particles in this study have a left skewness.

Table 4.2 Mode, Median and Span of lactose particle size distributions (mean ± SD, n=5)

| **Fraction** | **Mode (µm)** | **Median (µm)** | **Span** |
|---|---|---|---|
| 20-30 µm | 21.94 ± 2.35 | 18.21 ± 1.24 | 2.08 |
| 30-71 µm | 35.27 ± 0.83 | 29.11 ± 0.38 | 2.22 |
| 71-90 µm | 76.63 ± 1.85 | 64.97 ± 2.68 | 2.02 |

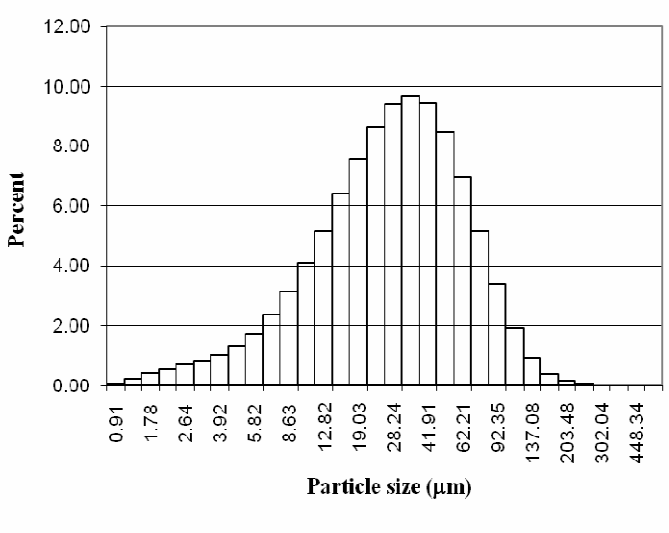


Figure 4.4 Particle size distribution of carrier collected from sieve 30-71 µm

### 4.2.2 Particle morphology of drug and carriers

Scanning electron micrographs show that the drug and carriers varied from irregular shapes to spherical shapes (Figure 4.5). Generally, pharmaceutical powders smaller than 5 µm are predicted to be able to enter the lower airways (Hickey, 1992). Figure 4.5 shows that micronized drugs have a particle size in a range of 1-5 µm while the collected lactose carriers have three size ranges. There is no readily distinguishable difference in the morphology of each collected lactose carrier. The fine drug particle and the remaining of fine lactose particle tended to be cohesive and formed agglomerates. While increasing of the lactose particle size, fine drug particles or fine lactose particles could distribute on the coarser particles surface by adhesive force. Figure 4.5 (E) shows mixed salbutamol sulfate with collected lactose from sieve size 30-71 µm have a good uniformity in the formulation.

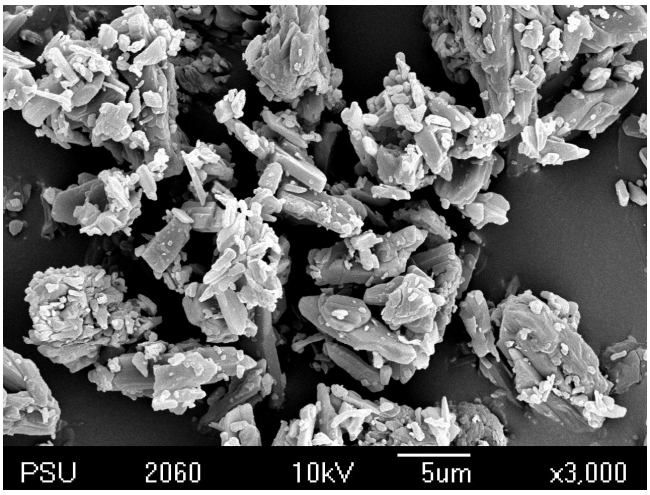


(A) Micronized salbutamol sulfate

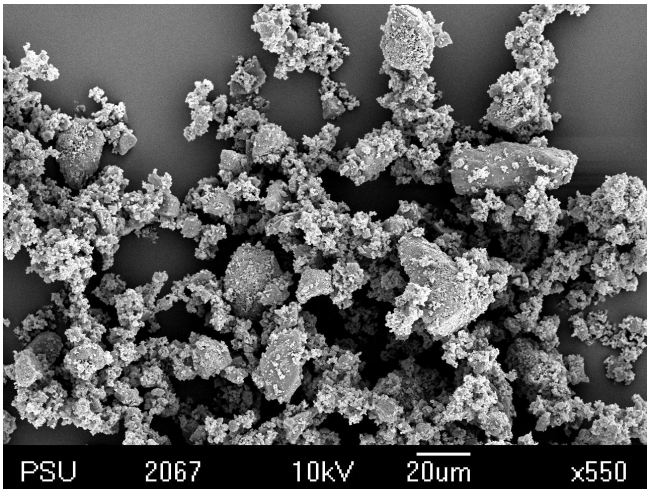


(B) Collected Lactose from sieve size 20-30 μm

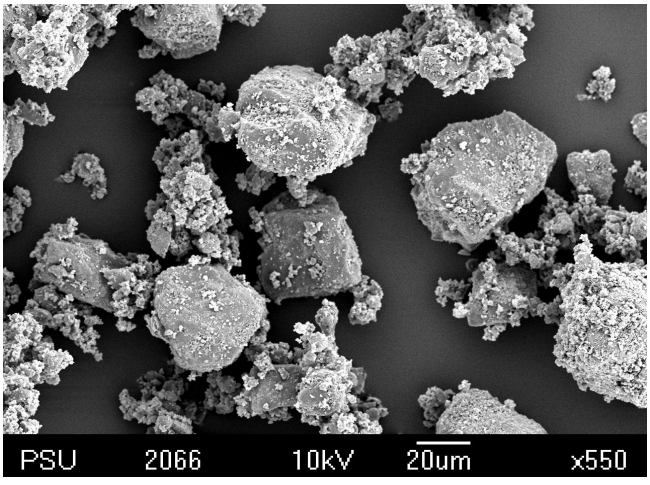


(C) Collected Lactose from sieve size 30-71 μm

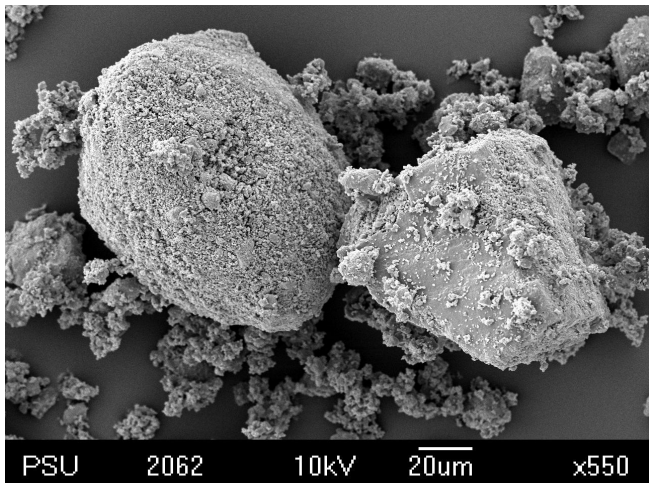


(D) Collected Lactose from sieve size 71-90 μm

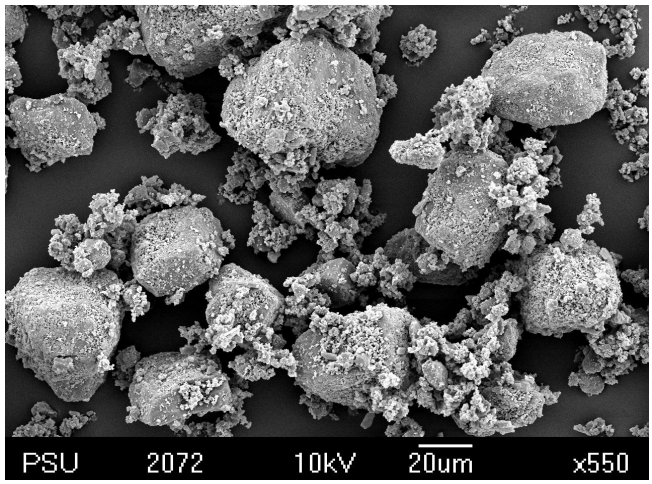


(E) Mixed salbutamol sulfate with collected lactose from sieve size 30-71 μm

Figure 4.5 Electron micrograph of (A) Micronized salbutamol sulfate, (B) Collected Lactose from sieve size 20-30 μm, (C) Collected Lactose from sieve size 30-71 μm, (D) Collected Lactose from sieve size 71-90 μm, (E) Mixed salbutamol sulfate with collected lactose from sieve size 30-71 μm

### 4.2.3 Content uniformity of dry powder formulations

After blending the carrier with salbutamol sulfate, the average content and the uniformity of drug were measured. Table 4.3 shows the content uniformity of all salbutamol sulfate formulations. All of three formulations have

very good content uniformity about 97 to 99%, with standard deviation less than two (Table 4.3). The results suggest that the overall process of mixing, sampling and analysis in this study was accurate and reproducible, and uniform mixing was achieved by employing this mixing procedure. In addition, the drug distribution in blends with all carriers was more homogeneous, probably because of its higher level of drug adhesion on the carrier and appropriate drug contents in dosage unit.

Table 4.3 Content uniformity of the salbutamol sulfate DPI formulations

| Dry powder formulations | Content Uniformity (Mean ± SD), n=5 |
|---|---|
| Formulation 1 (Salbutamol + Lactose 20-30 μm) | 97.87 ± 1.31 |
| Formulation 2 (Salbutamol + Lactose 30-71 μm) | 98.99 ± 0.81 |
| Formulation 3 (Salbutamol + Lactose 71-90 μm) | 98.66 ± 1.23 |

### 4.2.4 Dimensions of devices

From device cross section measurement, device shape, diameter, add-on and mouthpiece volume data are summarized in Table 4.4. All of commercial devices use either grid or impeller to increase particle-device impaction. Selected pipes have smallest internal diameter (about 3-5 μm) when compared with commercial device (about 5.5-16.5 μm) and have no impeller or grid inside device. When internal diameter and mouthpiece volume were compared among devices, results show internal diameter variation from 3 to 16 cm where as mouthpiece volumes are from less than 1 ml to 6 ml. Straight and curved pipes have longer internal mouthpiece distance than commercial devices.

Figure 4.6 shows dimensions of the selected tobacco pipes. The selected tobacco pipes have conical port for drug loading and have no impeller or grid inside. In this study, blister pack with loaded drug was placed on open-cone tip of pipes. The pin was pierce through of the blister wall and resulting in a release of drug from the blister through pipe inlet. In this study, the curved-pipe is expect to produce high turbulence air-flow through internal mouthpiece and could also reduce drug loss via inertial impaction.

Table 4.4 Cross section and device dimension data

| Device | Shape | Internal diameter (mm) | impeller | Grid | Mouthpiece Volume (ml) |
|---|---|---|---|---|---|
| Straight Pipe | Conical | 5.00 and 3.19 | No | No | 4.98 |
| Curved Pipe | Conical | 5.00 and 4.79 | No | No | 6.53 |
| Spinhaler® | Conical | 16.50 and 14.70 | Yes | No | 4.70 |
| Cyclohaler® | Cylindrical | 10.08 | No | Yes | 4.27 |
| Inhalator® | Cylindrical | 5.45 | No | Yes | 0.56 |

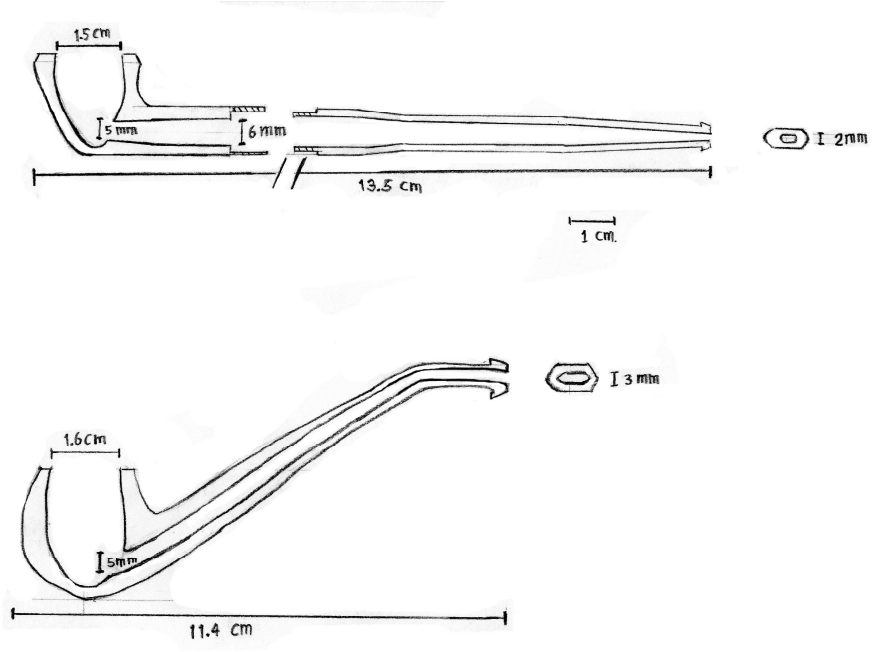


Figure 4.6 Dimensions of tobacco pipes

### 4.2.5 Device resistance of dry powder inhaler devices

The graph plot between flow rate and pressure drop shows relatively high pressure drop with higher device resistance (Figure 4.7). Calculated device resistance for Spinhaler, Cyclohaler, Inhalator, Straight and Curved pipes are 0.05, 0.08, 0.18, 0.39, 0.21 $(mbar^{1/2})$ /$(L\ min^{-1})$ respectively, reveals that “Spinhaler, Cyclohaler and Inhalator” are “low, medium and high” device resistance, respectively (Table 4.5). The values for specific resistance determined in this study are in general agreement with those presented in previous studies by Clark and Hollingworth (1993); De Boer et al. (1996). Straight and curved pipes can be classified as high device resistance. When consider to device diameter that two selected pipes have narrowest internal diameter. Results indicate that the device resistance has relative with the narrowest internal diameter appear on each device. Hence, the way to reduce device resistance on DPI devices is to increase the narrowest point of internal diameter in that device.

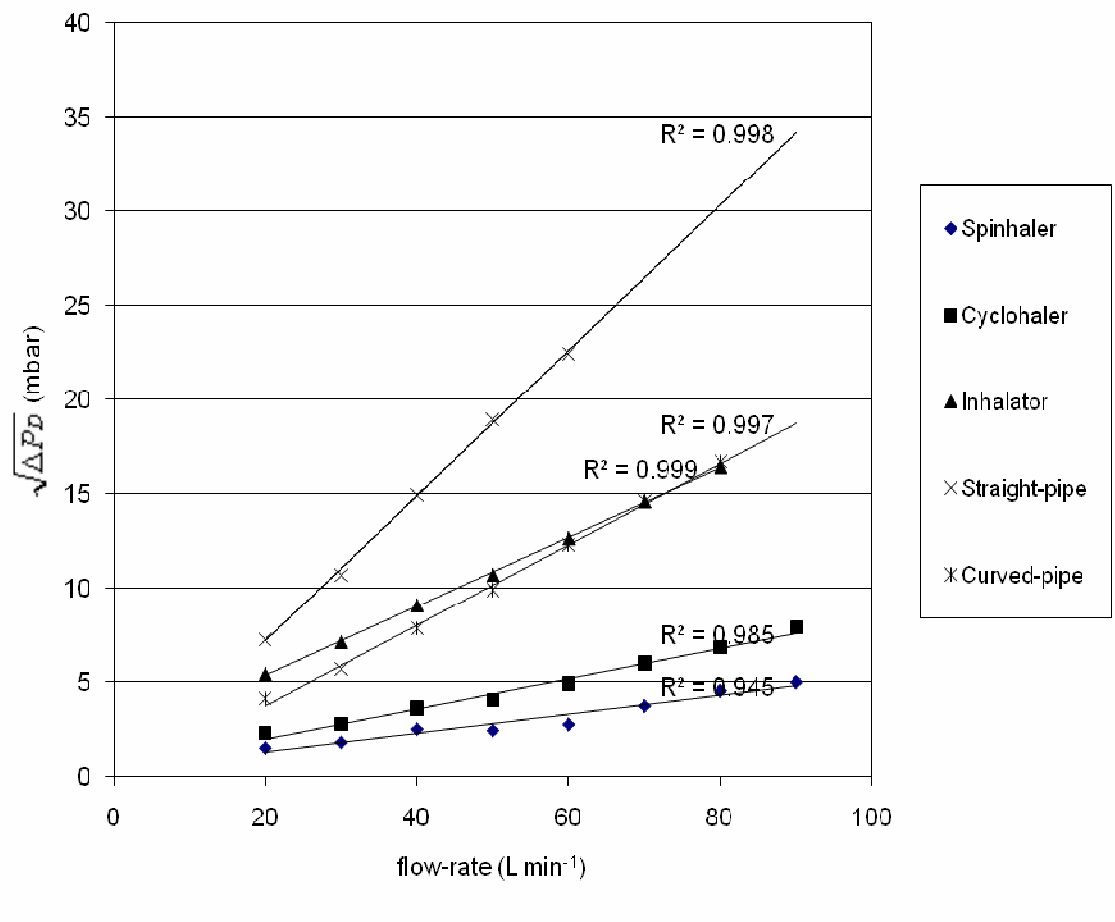


Figure 4.7 Relationships between square root pressure drop and flow-rate of DPI devices used in this study

Table 4.5 Device resistance of DPI device used in this study

| Device | Device resistance (mbar$^{1/2}$) /(L min$^{-1}$) |
|---|---|
| Spinhaler | 0.05 |
| Cyclohaler | 0.08 |
| Inhalator | 0.18 |
| Straight-pipe | 0.39 |
| Curved-pipe | 0.21 |

## 4.3 Devices performances

### 4.3.1 Drug emission

% emission from Formulations 1, 2, 3 delivered by all devices is shown in Figure 4.8. Percentage emission from these devices is about 80-90% of dose. There are no differences in each device, formulation and these three flow rates.

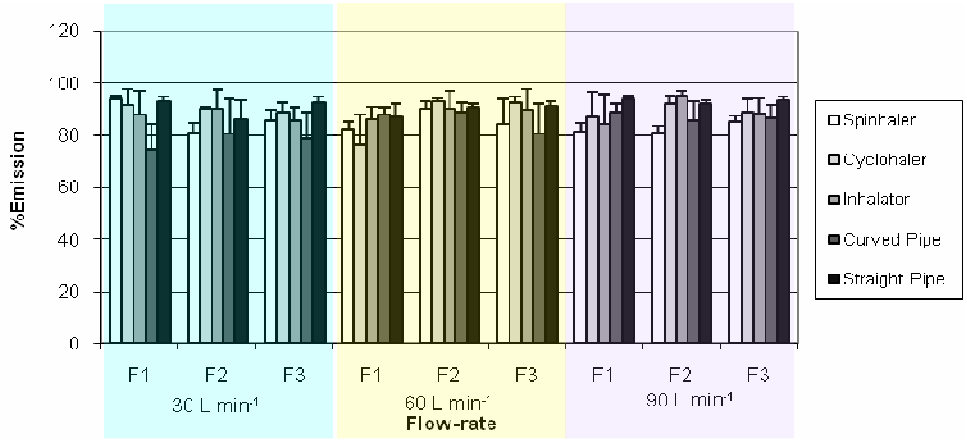


Figure 4.8 %Emissions from DPI devices with 3 formulations operating at 30, 60 and 90 L $min^{-1}$

### 4.3.2 Fine particle fraction

Increasing %FPF was obtained with higher flow rate as shown in Figure 4.9. The experimental data showed %FPF was trend related with operating flow-rate. The formulation 2 that containing carrier size ranges of 30-71 μm provided best performance especially at high flow rate, related to appropriate carrier particle size that has balance between adhesive and cohesive force between carrier and drug particles. While the other formulations

resulted with a bit lower of %FPF than the formulation 2 when consider within the same flow-rate. This is in line with the previous study by Louey et al. (2003).

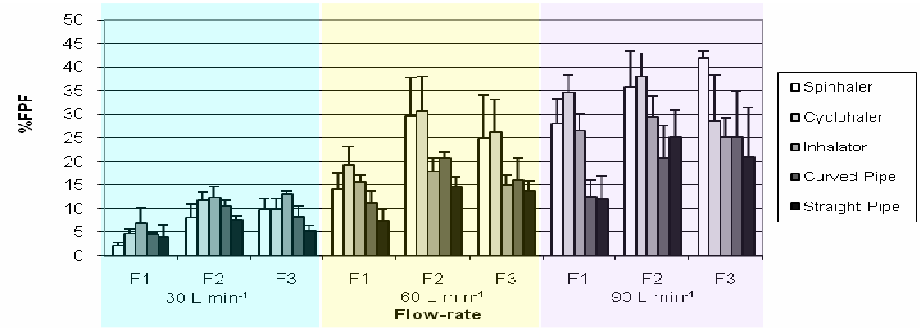


(a)

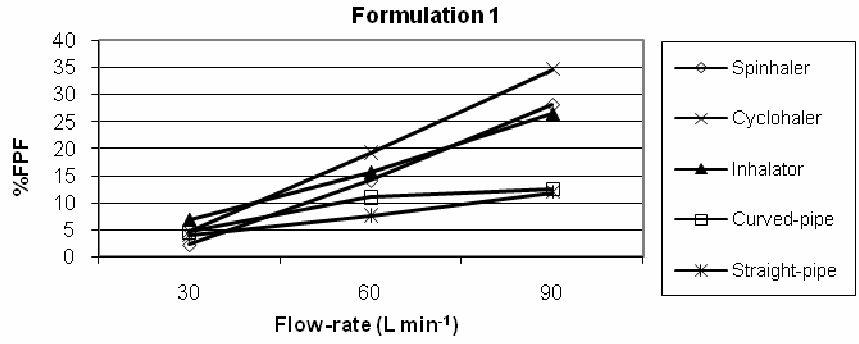


(b)

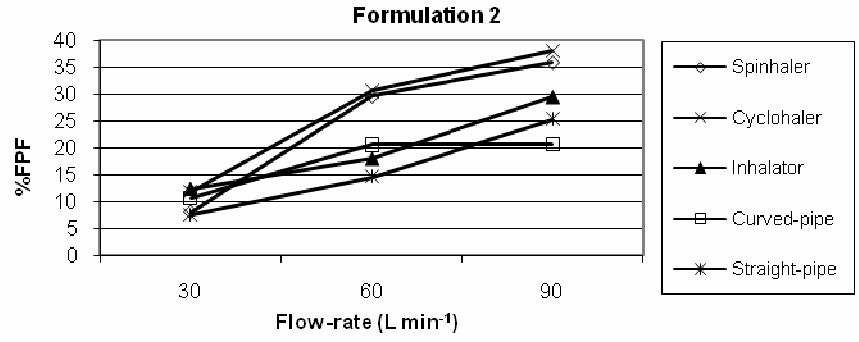


(c)

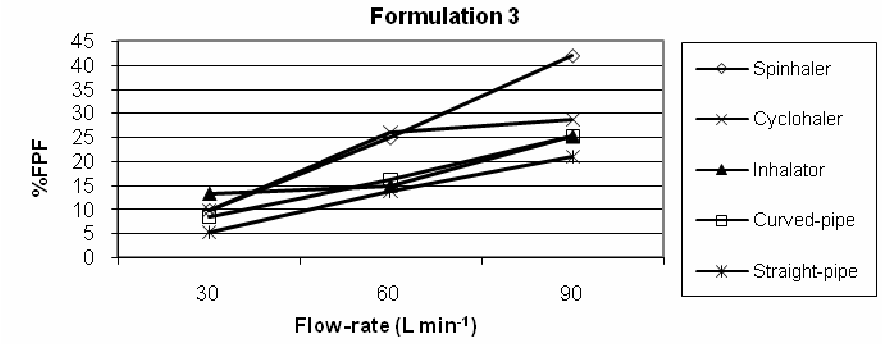


(d)

Figure 4.9 Calculated %FPF from DPI devices (a) with Formulation 1 (b), Formulation 2 (c) and Formulation 3 (d) operated at 30, 60 and 90 L $min^{-1}$

When we considered %FPF and flow rate in experimental device, Inhalator provide better %FPF at operated flow rate of 30 L $min^{-1}$. While operation at 60 and 90 L $min^{-1}$, low and medium device resistance (Spinhaler and Cyclohaler) increased %FPF much larger extent than that with high device resistance (Inhalator, Curved pipe and Straight pipe). Unchanged in %FPF found when operating flow-rate increased from 60 to 90 L $min^{-1}$ in curved-pipe with formulation 1 and 2. Results indicate that Spinhaler, Cyclohaler, Inhalator and Straight-pipe are flow-dependent device in terms of %FPF and Curved-pipe is flow-independent device. However, a clear relation between fine drug particle released and the device resistance in the delivery devices is not apparent from the figure. The cyclohaler is, by far, the device presenting the higher fine drug particle level, whereas the curved and the straight of the pipes exhibit the lowest values in the set. Surprisingly, it can be seen that the narrow of the air inlet of this device did not seem to produce any effect in such characteristic, as both versions of the pipes presented identical values of %FPF. An explanation for this observation may perhaps be found by assuming that the greater part of the turbulence in the exit air stream is generated by the grid located at the outlet of the chamber or the impeller inside device. The decrease in %FPF with high resistance devices can be due to the drug loss via inertial impaction (Table 4.6). When decreasing inlet diameter provide more air jet velocity from mouthpiece and increasing glass throat deposition. This is in line with the previous report (DeHaan and Finlay, 2004). The outlet diameter of device and formulations are two key factors to this incidence.

Table 4.6 Drug loss via inertial impaction (%nominal dose)

| Devices | outlet mouthpiece diameter (mm) | Drug loss in glass throat (%nominal dose) | | | | | | | | |
|---|---|---|---|---|---|---|---|---|---|---|
| | | Formulation 1 | | | Formulation 2 | | | Formulation 3 | | |
| | | 30 L $min^{-1}$ | 60 L $min^{-1}$ | 90 L $min^{-1}$ | 30 L $min^{-1}$ | 60 L $min^{-1}$ | 90 L $min^{-1}$ | 30 L $min^{-1}$ | 60 L $min^{-1}$ | 90 L $min^{-1}$ |
| Spinhaler | 14.70 | 50.50 | 31.53 | 36.34 | 36.14 | 28.20 | 30.90 | 37.52 | 29.64 | 30.87 |
| Cyclohaler | 10.08 | 40.19 | 31.11 | 39.47 | 29.21 | 35.98 | 40.40 | 35.40 | 35.54 | 48.28 |
| Inhalator | 5.45 | 38.55 | 43.81 | 50.86 | 40.10 | 49.25 | 51.26 | 36.75 | 52.00 | 55.09 |
| Curved-pipe | 4.79 | 57.96 | 51.81 | 70.44 | 48.00 | 35.52 | 61.04 | 48.71 | 41.44 | 49.92 |
| Straight-pipe | 3.19 | 63.78 | 68.78 | 69.64 | 50.87 | 57.67 | 43.16 | 60.40 | 59.82 | 60.13 |

### 4.3.3 Mass median aerodynamic diameter

MMADs were obtained in the range of 3-6 μm, and higher device resistance provided smaller MMADs (Figure 4.10). Only Spinhaler in formulation 1 and Curved pipe in formulation 3 that MMAD was slightly increased when flow-rate increased from 30 to 60 L $min^{-1}$. While operate from 60 to 90 L $min^{-1}$ only Spinhaler in formulation 2 and Straight pipe in formulation 3 showed slightly increase in MMAD. Otherwise, the MMAD was generally decreased while operable at higher flow-rate. Results indicate that increasing degree of turbulence air-flow through device by increase operating flow-rate or device resistance also can decrease in generated of drug MMAD.

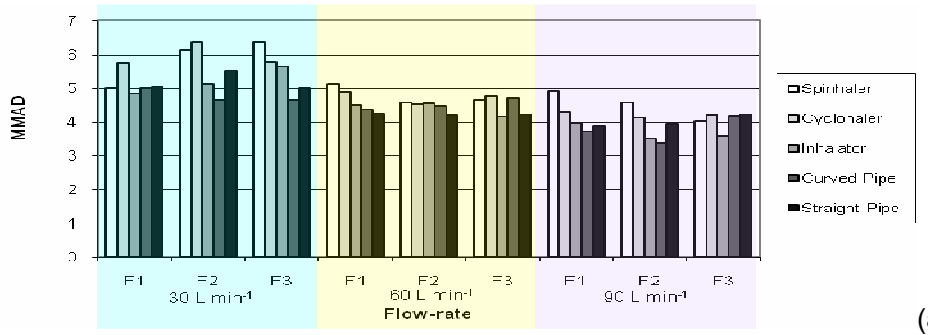


(a)

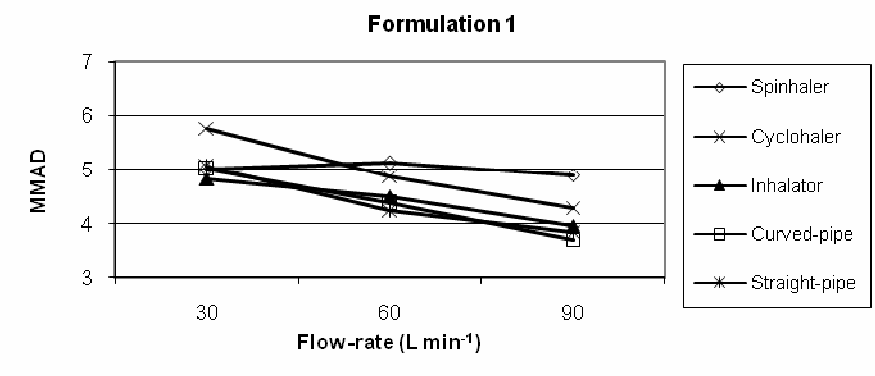


(b)

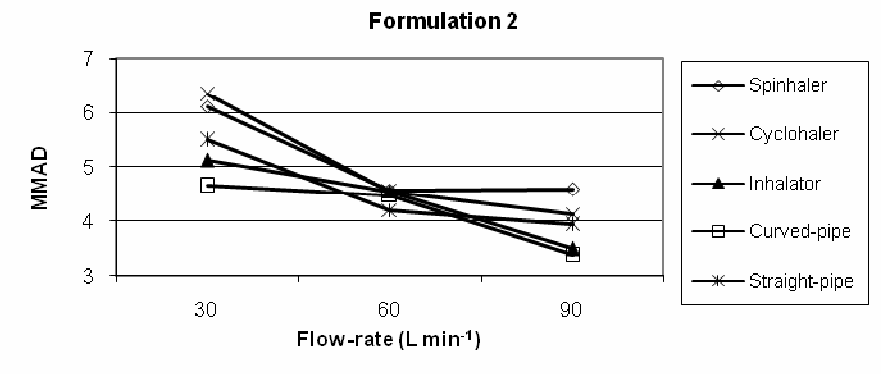


(c)

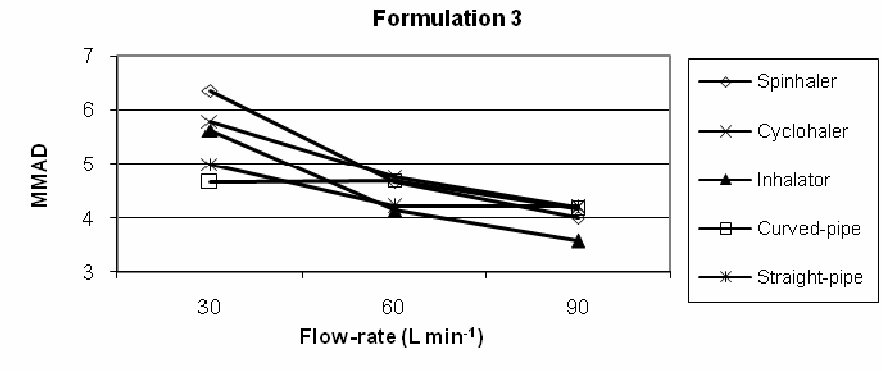


(d)

Figure 4.10 Calculated MMAD from DPI devices (a) with Formulation 1 (b), Formulation 2 (c) and Formulation 3 (d) operated at 30, 60 and 90 L $min^{-1}$

### 4.3.4 Modeling of air-flow through pipes device

Meshing was exported from Gambit which contained a total of 6894 nodes and 28295 elements for straight-pipe and a total of 7832 nodes and 34700 elements for curved-pipe. Because of the calculated pressure solved from Fluent must be compared with pressure drop from experiment and the limited of program that cannot be solved well enough for required when calculated at lower flow-rate condition. The solution from Fluent must be calculated from the maximum flow-rate available in device resistance evaluation, for straight-pipe at 60 L $min^{-1}$ and curved-pipe at 80 L $min^{-1}$. Figure 4.11 shows that calculated maximum dynamic pressure for curved-pipe is 244.50 mbar and straight-pipe is 193.23 mbar while experimental data are 401.33 and 250.67 mbar by order. In order to compare the results in this study with pressure drop values in mbar, we have to converse all pressure values in pascal to mbar which one pascal is equal to 0.01 mbar. The pressure drop calculated from Fluent is close to the experiment results. Thus, the designed model is valid. We also used Reynolds number inside pipe devices to compare between two pipes. Figure 4.12 shows cell Reynolds number calculated from 80 L $min^{-1}$ and the velocity of air-flow through both devices. Results show that Reynolds number range from 3.43 to 8316.74 for curved-pipe and from 22.99 to 13087.66 for straight-pipe. When we consider in graphic displays that divided Reynolds number into color, results show that higher degree of Reynolds number provide just only at the tip of mouthpiece for straight-pipe whereas for the curved-pipe it spread's along the mouthpiece. When color graphic was considered along devices, it illustrated that average of Reynolds number through curved-pipe was higher than the straight-pipe. Results indicate that curved-pipe provides lower device resistance than straight-pipe however the curved shape design from curved-pipe could provide more turbulence air-flow.

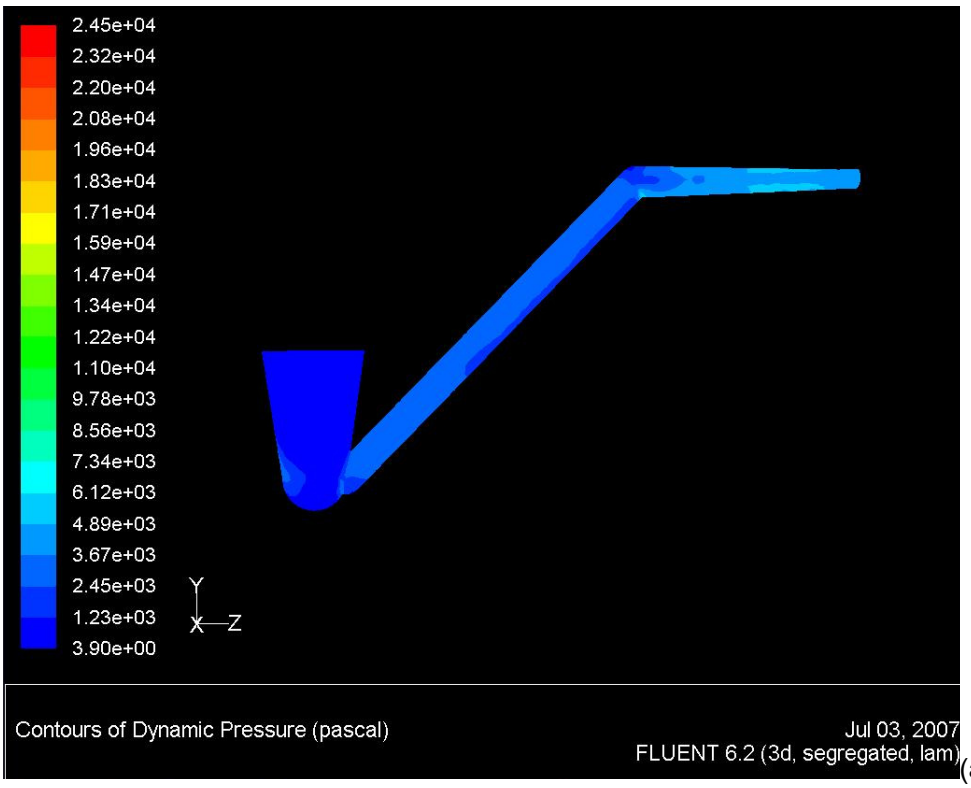


(a)

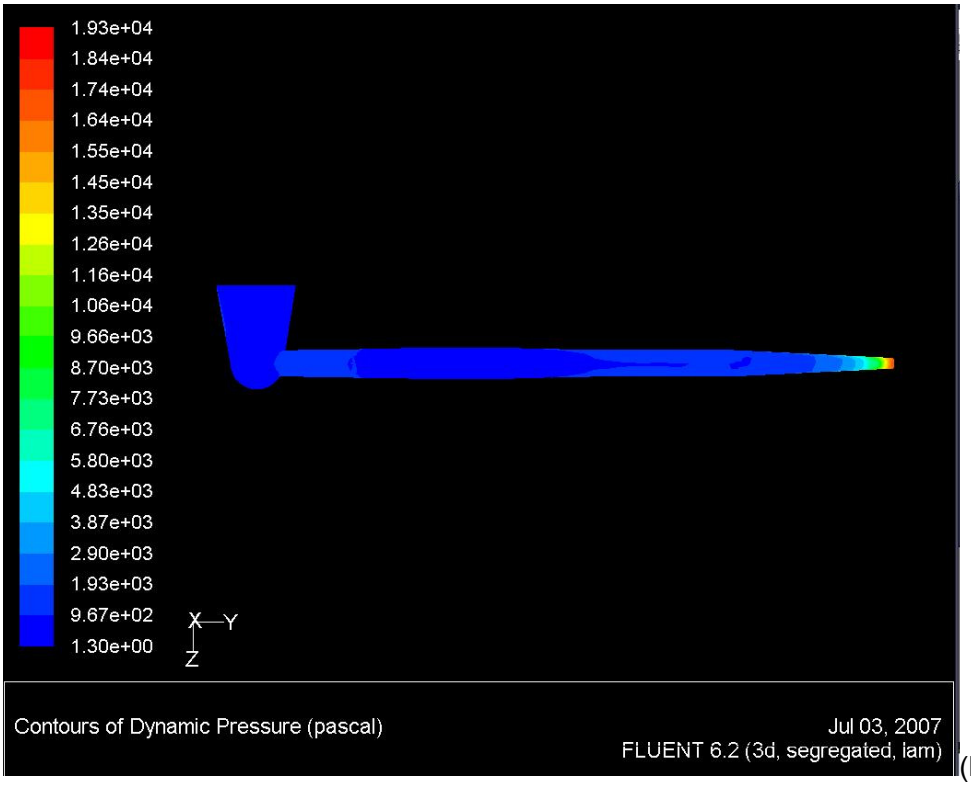


(b)

Figure 4.11 Calculated dynamic pressure (pascal) of curved pipe (a) and straight pipe (b)

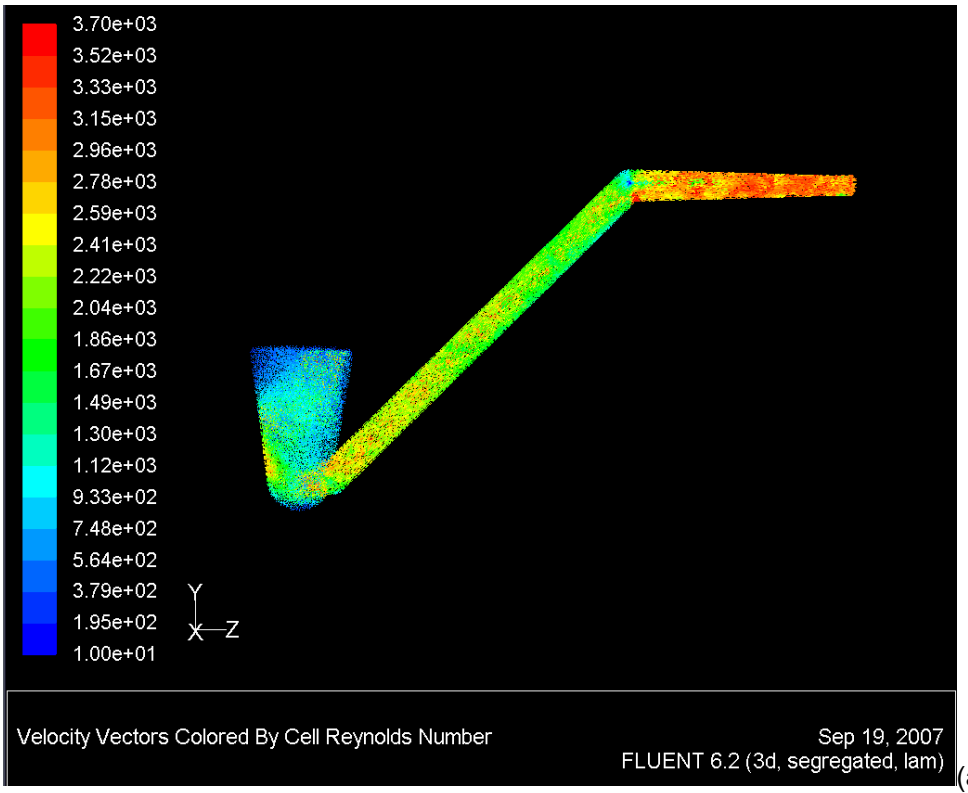

(a)

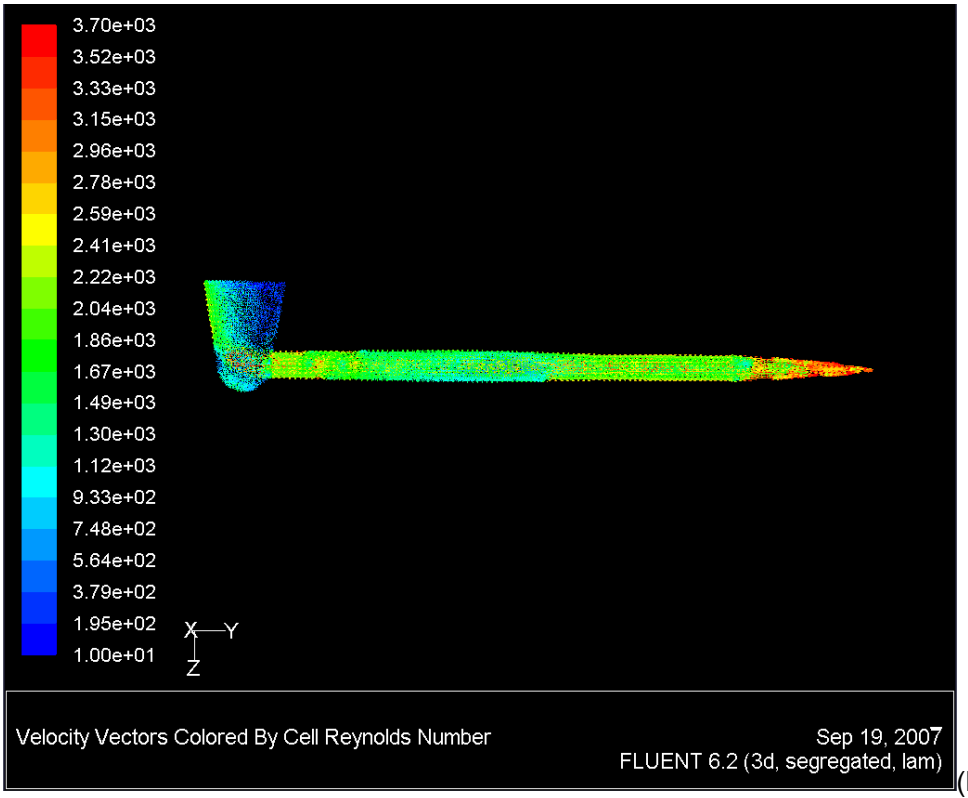

(b)

Figure 4.12 Calculated cell Reynolds number and velocity vectors of curved pipe (a) and straight pipe (b)